1-1-2012

# Measurement of Exclusive π0 Electroproduction Structure Functions and their Relationship to Transverse Generalized Parton Distributions

I. Bedlinshy

Angela Biselli
*Fairfield University*, abiselli@fairfield.edu

CLAS Collaboration



**Peer Reviewed**



## Published Citation

I. Bedlinshy, et al. [CLAS Collaboration]. "Measurement of Exclusive π0 Electroproduction Structure Functions and their Relationship to Transverse Generalized Parton Distributions," Physical Review Letters. 109.11 (2012) DOI: 10.1103/PhysRevLett.109.112001

# Measurement of Exclusive $\pi^0$ Electroproduction Structure Functions and their Relationship to Transverse Generalized Parton Distributions

I. Bedlinskiy,[22] V. Kubarovsky,[35,30] S. Niccolai,[21] P. Stoler,[30] K. P. Adhikari,[29] M. Aghasyan,[18] M. J. Amaryan,[29] M. Anghinolfi,[19] H. Avakian,[35] H. Baghdasaryan,[39,41] J. Ball,[7] N. A. Baltzell,[1] M. Battaglieri,[19] R. P. Bennett,[29] A. S. Biselli,[11,30] C. Bookwalter,[13] S. Boiarinov,[35] W. J. Briscoe,[15] W. K. Brooks,[37,35] V. D. Burkert,[35] D. S. Carman,[35] A. Celentano,[19] S. Chandavar,[28] G. Charles,[7] M. Contalbrigo,[17] V. Crede,[13] A. D'Angelo,[20,32] A. Daniel,[28] N. Dashyan,[41] R. De Vita,[19] E. De Sanctis,[18] A. Deur,[35] C. Djalali,[34] D. Doughty,[8,35] R. Dupre,[7] H. Egiyan,[35,40] A. El Alaoui,[1] L. El Fassi,[1] L. Elouadrhiri,[35] P. Eugenio,[13] G. Fedotov,[34] S. Fegan,[38] J. A. Fleming,[10] T. A. Forest,[16] A. Fradi,[21] M. Garçon,[7] N. Gevorgyan,[41] K. L. Giovanetti,[23] F. X. Girod,[35] W. Gohn,[9] R. W. Gothe,[34] L. Graham,[34] K. A. Griffioen,[40] B. Guegan,[21] M. Guidal,[21] L. Guo,[12,35] K. Hafidi,[1] H. Hakobyan,[37,41] C. Hanretty,[39] D. Heddle,[8,35] K. Hicks,[28] M. Holtrop,[26] Y. Ilieva,[34,15] D. G. Ireland,[38] B. S. Ishkhanov,[33] E. L. Isupov,[33] H. S. Jo,[21] K. Joo,[9] D. Keller,[39] M. Khandaker,[27] P. Khetarpal,[12] A. Kim,[24] W. Kim,[24] F. J. Klein,[6] S. Koirala,[29] A. Kubarovsky,[30,33] S. E. Kuhn,[29] S. V. Kuleshov,[37,22] N. D. Kvaltine,[39] K. Livingston,[38] H. Y. Lu,[5] I. J. D. MacGregor,[38] Y. Mao,[34] N. Markov,[9] D. Martinez,[16] M. Mayer,[29] B. McKinnon,[38] C. A. Meyer,[5] T. Mineeva,[9] M. Mirazita,[18] V. Mokeev,[35,33] H. Moutarde,[7] E. Munevar,[35] C. Munoz Camacho,[21] P. Nadel-Turonski,[35] G. Niculescu,[23,28] I. Niculescu,[23,35] M. Osipenko,[19] A. I. Ostrovidov,[13] L. L. Pappalardo,[17] R. Paremuzyan,[41,*] K. Park,[35,24] S. Park,[13] E. Pasyuk,[35,2] S. Anefalos Pereira,[18] E. Phelps,[34] S. Pisano,[18] O. Pogorelko,[22] S. Pozdniakov,[22] J. W. Price,[3] S. Procureur,[7] Y. Prok,[8,39] D. Protopopescu,[38,26] A. J. R. Puckett,[35] B. A. Raue,[12,35] G. Ricco,[14,†] D. Rimal,[12] M. Ripani,[19] G. Rosner,[38] P. Rossi,[18] F. Sabatié,[7] M. S. Saini,[13] C. Salgado,[27] N. Saylor,[30] D. Schott,[12] R. A. Schumacher,[5] E. Seder,[9] H. Seraydaryan,[29] Y. G. Sharabian,[35] G. D. Smith,[38] D. I. Sober,[6] D. Sokhan,[21] S. S. Stepanyan,[35] S. Stepanyan,[35] S. Strauch,[34,15] M. Taiuti,[14,†] W. Tang,[28] C. E. Taylor,[16] Ye Tian,[34] S. Tkachenko,[39] M. Ungaro,[35,30] M. F. Vineyard,[36,31] A. Vlassov,[22] H. Voskanyan,[41] E. Voutier,[25] N. K. Walford,[6] D. P. Watts,[10] L. B. Weinstein,[29] D. P. Weygand,[35] M. H. Wood,[4,34] N. Zachariou,[34] J. Zhang,[35] Z. W. Zhao,[39] and I. Zonta[20,‡]

(CLAS Collaboration)

[1]*Argonne National Laboratory, Argonne, Illinois 60439, USA*
[2]*Arizona State University, Tempe, Arizona 85287-1504, USA*
[3]*California State University, Dominguez Hills, Carson, California 90747, USA*
[4]*Canisius College, Buffalo, New York, USA*
[5]*Carnegie Mellon University, Pittsburgh, Pennsylvania 15213, USA*
[6]*Catholic University of America, Washington, D.C. 20064, USA*
[7]*CEA, Centre de Saclay, Irfu/Service de Physique Nucléaire, 91191 Gif-sur-Yvette, France*
[8]*Christopher Newport University, Newport News, Virginia 23606, USA*
[9]*University of Connecticut, Storrs, Connecticut 06269, USA*
[10]*Edinburgh University, Edinburgh EH9 3JZ, United Kingdom*
[11]*Fairfield University, Fairfield Connecticut 06824, USA*
[12]*Florida International University, Miami, Florida 33199, USA*
[13]*Florida State University, Tallahassee, Florida 32306, USA*
[14]*Università di Genova, 16146 Genova, Italy*
[15]*The George Washington University, Washington, D.C. 20052, USA*
[16]*Idaho State University, Pocatello, Idaho 83209, USA*
[17]*INFN, Sezione di Ferrara, 44100 Ferrara, Italy*
[18]*INFN, Laboratori Nazionali di Frascati, 00044 Frascati, Italy*
[19]*INFN, Sezione di Genova, 16146 Genova, Italy*
[20]*INFN, Sezione di Roma Tor Vergata, 00133 Rome, Italy*
[21]*Institut de Physique Nucléaire ORSAY, Orsay, France*
[22]*Institute of Theoretical and Experimental Physics, Moscow, 117259, Russia*
[23]*James Madison University, Harrisonburg, Virginia 22807, USA*
[24]*Kyungpook National University, Daegu 702-701, Republic of Korea*
[25]*LPSC, Universite Joseph Fourier, CNRS/IN2P3, INPG, Grenoble, France*
[26]*University of New Hampshire, Durham, New Hampshire 03824-3568, USA*
[27]*Norfolk State University, Norfolk, Virginia 23504, USA*
[28]*Ohio University, Athens, Ohio 45701, USA*

 

[29]Old Dominion University, Norfolk, Virginia 23529, USA
[30]Rensselaer Polytechnic Institute, Troy, New York 12180-3590, USA
[31]University of Richmond, Richmond, Virginia 23173, USA
[32]Universita' di Roma Tor Vergata, 00133 Rome Italy
[33]Skobeltsyn Nuclear Physics Institute, 119899 Moscow, Russia
[34]University of South Carolina, Columbia, South Carolina 29208, USA
[35]Thomas Jefferson National Accelerator Facility, Newport News, Virginia 23606, USA
[36]Union College, Schenectady, New York 12308, USA
[37]Universidad Técnica Federico Santa María, Casilla 110-V Valparaíso, Chile
[38]University of Glasgow, Glasgow G12 8QQ, United Kingdom
[39]University of Virginia, Charlottesville, Virginia 22901, USA
[40]College of William and Mary, Williamsburg, Virginia 23187-8795, USA
[41]Yerevan Physics Institute, 375036 Yerevan, Armenia
(Received 13 June 2012; published 10 September 2012)

Exclusive $\pi^0$ electroproduction at a beam energy of 5.75 GeV has been measured with the Jefferson Lab CLAS spectrometer. Differential cross sections were measured at more than 1800 kinematic values in $Q^2$, $x_B$, $t$, and $\phi_\pi$, in the $Q^2$ range from 1.0 to 4.6 GeV$^2$, $-t$ up to 2 GeV$^2$, and $x_B$ from 0.1 to 0.58. Structure functions $\sigma_T + \epsilon\sigma_L$, $\sigma_{TT}$, and $\sigma_{LT}$ were extracted as functions of $t$ for each of 17 combinations of $Q^2$ and $x_B$. The data were compared directly with two handbag-based calculations including both longitudinal and transversity generalized parton distributions (GPDs). Inclusion of only longitudinal GPDs very strongly underestimates $\sigma_T + \epsilon\sigma_L$ and fails to account for $\sigma_{TT}$ and $\sigma_{LT}$, while inclusion of transversity GPDs brings the calculations into substantially better agreement with the data. There is very strong sensitivity to the relative contributions of nucleon helicity-flip and helicity nonflip processes. The results confirm that exclusive $\pi^0$ electroproduction offers direct experimental access to the transversity GPDs.

DOI: 10.1103/PhysRevLett.109.112001 PACS numbers: 13.60.Le, 14.20.Dh, 14.40.Be, 24.85.+p

A major goal of hadronic physics is to describe the three dimensional structure of the nucleon in terms of its quark and gluon fields. Deep inelastic scattering experiments have provided a large body of information about quark longitudinal momentum distributions. Exclusive electron scattering experiments, in which all final-state particles are measured, have been rather successfully analyzed and interpreted by Regge models which are based on hadronic degrees of freedom (see, for example, Refs. [1,2]). However, during the past decade the handbag mechanism has become the leading theoretical approach for extracting the nucleon quark and gluon structure from exclusive reactions such as deeply virtual Compton scattering (DVCS) and deeply virtual meson electroproduction. In this approach, the quark distributions are parametrized in terms of generalized parton distributions (GPDs). The GPDs contain information about the distributions of both the longitudinal momentum and the transverse position of partons in the nucleon. In the handbag mechanism, the reaction amplitude factorizes into two parts. One part describes the basic hard electroproduction process with a parton within the nucleon, and the other—the GPD—contains the distribution of partons within the nucleon which are the result of soft processes. While the former is reaction dependent, the latter is a universal property of the nucleon structure common to the various exclusive reactions. This is schematically illustrated in Fig. 1. While the handbag mechanism should be most applicable at asymptotically large photon virtuality $Q^2$, DVCS experiments at $Q^2$ as low as 1.5 GeV$^2$ appear to be described rather well at a leading twist by the handbag mechanism, while the range of validity of leading order applicability of deeply virtual meson electroproduction is not as clearly determined.

There are eight GPDs. Four correspond to parton helicity conserving (chiral-even) processes, denoted by $H^q$, $\tilde{H}^q$, $E^q$, and $\tilde{E}^q$. Four correspond to parton helicity-flip (chiral-odd) processes [3,4], $H_T^q$, $\tilde{H}_T^q$, $E_T^q$, and $\tilde{E}_T^q$. The GPDs depend on three kinematic variables: $x$, $\xi$, and $t$, where $x$ is the average parton longitudinal momentum fraction and $\xi$ (skewness) is half of the longitudinal momentum fraction

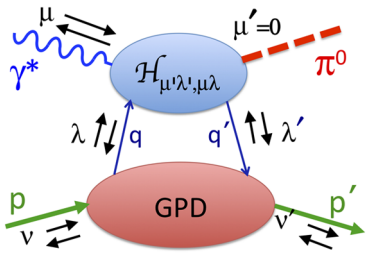


FIG. 1 (color online). Schematic diagram of the $\pi^0$ electroproduction amplitude in the framework of the handbag mechanism. The helicities of the initial and final nucleons are denoted by $\nu$ and $\nu'$, the incident photon and produced meson by $\mu$ and $\mu'$, and the active initial and final quark by $\lambda$ and $\lambda'$. The arrows in the figure represent the corresponding helicities.

transferred to the struck parton. The skewness can be expressed in terms of the Bjorken variable $x_B$ as $\xi \simeq x_B/(2-x_B)$, in which $x_B = Q^2/(2p\cdot q)$, $q$ is the four-momentum of the virtual photon, and $Q^2 = -q^2$. The momentum transfer to the nucleon is $t = (p - p')^2$, where $p$ and $p'$ are the initial and final four momenta of the nucleon.

In the forward limit where $t \to 0$, $H^q$ and $\tilde{H}^q$ reduce to the parton density distributions $q(x)$ and parton helicity distributions $\Delta q(x)$, respectively. The first moments in $x$ of the chiral-even GPDs are related to the elastic form factors of the nucleon: the Dirac form factor $F_1^q(t)$, the Pauli form factor $F_2^q(t)$, the axial-vector form factor $g_A^q(t)$, and the pseudoscalar form factor $h_A^q(t)$ [5].

Most of the reactions studied, such as DVCS or vector meson production, are at leading order primarily sensitive to the chiral-even GPDs. Very little is known about the chiral-odd GPDs. $H_T^q$ becomes the transversity function $h_1^q(x)$ in the forward limit. The chiral-odd GPDs are difficult to access since subprocesses with a quark helicity flip are suppressed. However, a complete description of nucleon structure requires the knowledge of the transversity GPDs as well as chiral-even GPDs.

Pseudoscalar meson electroproduction, and in particular $\pi^0$ production in the reaction $ep \to e'p'\pi^0$, was identified [6,7] as especially sensitive to the helicity-flip subprocesses. Evidence of their possible contribution to $\pi^+$ electroproduction in target spin asymmetry data [8] was noted in Ref. [7]. A disadvantage of $\pi^+$ production is that the interpretation is complicated by the dominance of the longitudinal $\pi^+$-pole term, which is absent in $\pi^0$ production. In addition, for $\pi^0$ production the structure of the amplitudes further suppresses the quark helicity conserving amplitudes relative to the helicity-flip amplitudes [7]. On the other hand, $\pi^0$ cross sections over a large kinematic range are much more difficult to obtain than for $\pi^+$ for two reasons: First, the cross sections are much smaller than for $\pi^+$, and second, the clean detection of $\pi^0$'s requires the measurement of their two decay photons.

This Letter presents the results of a measurement of $\pi^0$ electroproduction cross sections. The primary focus here is in its interpretation within the framework of the handbag model and on its sensitivity, within this framework, of accessing the quark helicity-flip GPDs.

The handbag mechanism is schematically illustrated in Fig. 1. The reaction can be written as a linear sum of amplitudes, each of which factorizes into two processes. In the framework of Ref. [4] we note the following: (1) A process in which the incident virtual photon of helicity $\mu = 0, \pm 1$ interacts with a single quark within the nucleon having a momentum fraction $x + \xi/2$ and helicity $\lambda = \pm 1/2$, to produce a meson with helicity $\mu' = 0$ and a returning quark with momentum fraction $x - \xi/2$ and helicity $\lambda' = \pm 1/2$, which is absorbed to form the final nucleon. In the present study for transversely polarized photons $\lambda' = -\lambda$, $\mu = \pm 1$, and $\nu' = \pm\nu$. (2) Process 1 is convoluted with a GPD, which encodes the distribution of quark and gluon longitudinal momentum fractions and transverse spatial distributions within the nucleon.

The primary contributing GPDs in meson production for transverse photons are $H_T$, which characterizes the quark distributions involved in nucleon helicity flip, and $\bar{E}_T (= 2\tilde{H}_T + E_T)$, which characterizes the quark distributions involved in nucleon non-helicity-flip processes [9,10]. This GPD describes the density of transversely polarized quarks in an unpolarized nucleon [9,10].

The relative contributions of the nucleon helicity-flip and nucleon helicity nonflip processes determine the $t$ dependence of the differential cross sections.

Exclusive $\pi^0$ electroproduction was measured at Jefferson Lab with the CLAS large acceptance spectrometer [11]. Cross sections were extracted over a wide range in $Q^2$, $t$, $x_B$, and $\phi_\pi$ (the azimuthal angle of the pion production plane relative to the electron scattering plane). The incident electron beam energy was 5.75 GeV. The target was liquid hydrogen of length 2.5 cm. The integrated luminosity was 20 fb$^{-1}$. The CLAS detector consists of six identical sectors within a toroidal magnetic field. Each sector is equipped with three layers of drift chambers to determine the trajectory of charged particles, a gas Cherenkov counter for electron identification, a scintillation hodoscope for time-of-flight measurement, and an electromagnetic calorimeter for electron identification and photon detection for angles greater than 21°. A forward angle calorimeter was added to the standard CLAS configuration downstream of the target for the detection of pion decay photons in the forward direction (4.5° to 15°). A superconducting solenoid around the target was used to trap Moller electrons along the beam axis, while permitting detection of photons starting at 4.5°, protons in the range 21° to 60°, and electrons from 21° to 45°. All four final-state particles of the reaction $ep \to e'p'\pi^0$, $\pi^0 \to \gamma\gamma$ were detected.

The kinematic requirements for the accepted data were $Q^2 \geq 1$ GeV$^2$, center-of-mass energy $W \geq 2$ GeV, and scattered electron energy $E' \geq 0.8$ GeV. The corresponding range of $x_B$ was from 0.1 to 0.58. The electrons were identified by requiring both a Cherenkov signal and an appropriate energy deposition in the electromagnetic calorimeter. Protons were identified by TOF measurement. Geometric cuts were applied to include only regions of the detector with well-understood acceptance and efficiency, as well as electron and proton target vertex position cuts, to ensure well-identified events.

The photons from $\pi^0 \to \gamma\gamma$ decays were detected in the electromagnetic calorimeters. Once all final particles were identified, the exclusive reaction $ep \to e'p'\pi^0$ was selected as follows: The angle between the direction of the reconstructed $\pi^0$'s and the missing momentum for $ep \to e'p'X$ had to be less than 2°. $3\sigma$ cuts were made on the missing mass $M_X^2(ep \to e'p'X) = m_{\pi^0}^2$, the missing mass

$M_X(ep \to e'\gamma\gamma X) = M_p$, the missing energy $E_X(ep \to e'p'\pi^0) = 0$, and the invariant mass $M_{\gamma\gamma} = m_{\pi^0}$. The background under the $\pi^0$ invariant mass peak, typically 3 to 5%, was subtracted using the data in the sidebands.

Corrections for the inefficiencies in track reconstruction and detector inefficiencies were applied. The acceptance was calculated using the standard GEANT3-based CLAS Monte Carlo simulation software. The Monte Carlo generator for exclusive $\pi^0$ electroproduction was parametrized to be consistent with the data. The ratio of the number of reconstructed Monte Carlo events to the data events was typically a factor of about 12. Thus, the statistical error introduced by the acceptance calculation was much smaller than for the data.

The data were binned in $Q^2$, $x_B$, $t$, and $\phi_\pi$, and differential cross sections $d^4\sigma/dQ^2dx_Bdtd\phi_\pi$ were obtained for more than 1800 bins.

Radiative corrections were calculated using the software package EXCLURAD [12], which had been previously developed and used for analyzing earlier CLAS $\pi^0$ experiments. Radiative corrections depend on $Q^2$, $t$, $x_B$, and $\phi_\pi$. They vary from 5% to 10%, depending on the kinematics.

An overall normalization factor of 1.12 was obtained from comparing elastic cross sections requiring $e$-$p$ coincidence, with published data. A systematic uncertainty of $\pm 6\%$ was applied to the resulting cross sections due to this correction.

Other systematic uncertainty studies included the electron, proton, and photon particle identification, the variation of the cuts on missing masses $M_X(ep \to e'\gamma\gamma X)$ and $M_X(ep \to e'p'X)$, missing energy, fiducial volumes, invariant mass $M_{\gamma\gamma}$, and radiative corrections. The overall systematic uncertainties were estimated at about 10%.

The structure functions are related to the differential cross sections by [7]

$$\frac{d^4\sigma}{dQ^2dx_Bdtd\phi_\pi} = \Gamma(Q^2, x_B, E)\frac{1}{2\pi}[\sigma_T + \epsilon\sigma_L + \epsilon\cos 2\phi_\pi\sigma_{TT} + \sqrt{2\epsilon(1+\epsilon)}\cos\phi_\pi\sigma_{LT}]. \quad (1)$$

The Hand convention [13] was adopted for the definition of the virtual photon flux factor $\Gamma$. The unseparated cross section $\sigma_U = \sigma_T + \epsilon\sigma_L$, and the interference terms $\sigma_{LT}$ and $\sigma_{TT}$ were extracted from the $\cos\phi_\pi$ and $\cos 2\phi_\pi$ dependences of the cross sections. The extracted structure functions as functions of $-t$ are presented in Fig. 2 for 6 of the 17 bins in $Q^2$ and $x_B$ bins, which have the largest kinematic coverage and for which there are theoretical calculations. A recent experiment, Ref. [14], measured $\pi^0$ cross sections in a limited kinematic range. When their results are projected to the present $Q^2$ the unseparated cross sections agree within a few percent.

The results of two GPD-based models [15,16] are superimposed in Fig. 2. The contributions from transversely polarized photons are primarily from $H_T$ and $\bar{E}_T$. Reference [15] obtains the following relations:

$$\sigma_T = \frac{4\pi\alpha_e}{2\kappa}\frac{\mu_\pi^2}{Q^4}[(1-\xi^2)|\langle H_T\rangle|^2 - \frac{t'}{8m^2}|\langle\bar{E}_T\rangle|^2] \quad (2)$$

and

$$\sigma_{TT} = \frac{4\pi\alpha_e}{2\kappa}\frac{\mu_\pi^2}{Q^4}\frac{t'}{8m^2}|\langle\bar{E}_T\rangle|^2. \quad (3)$$

Here $\kappa(Q^2, x_B)$ is a phase space factor, $t' = t - t_{\min}$, and the brackets $\langle H_T\rangle$ and $\langle\bar{E}_T\rangle$ denote the convolution of the elementary process with the GPDs $H_T$ and $\bar{E}_T$.

The contribution $\sigma_L$ accounts for only a small fraction in both calculations (typically less than a few percent) of the unseparated $\sigma_T + \epsilon\sigma_L$ in the kinematic regime under investigation. This is because $\tilde{H}$ and $\tilde{E}$, the GPDs which are responsible for the leading-twist structure function $\sigma_L$, are very small. This is not the case for $\bar{E}_T$ and $H_T$ which contribute to $\sigma_T$ and $\sigma_{TT}$. In addition, the transverse cross sections are strongly enhanced by the chiral condensate through the parameter $\mu_\pi = m_\pi^2/(m_u + m_d)$, where $m_u$ and $m_d$ are current quark masses [7].

With the inclusion of the quark helicity nonconserving chiral-odd GPDs, which contribute primarily to $\sigma_T$ and $\sigma_{TT}$ and, to a lesser extent $\sigma_{LT}$, the model agrees moderately well with the data. Deviations in shape become greater at smaller $t'$ for the unseparated cross section $\sigma_U$. The behavior of the cross section near the threshold $t'$ is determined by the interplay between $H_T$ and $\bar{E}_T$. If $\bar{E}_T$ dominates, the cross section becomes small as $t' \to 0$. For the GPDs of Ref. [15], the parametrization was guided by the lattice calculation results of Ref. [10], while Ref. [16] used a GPD Reggeized diquark-quark model to obtain the GPDs. The results in Fig. 2 for the model of Ref. [15] (solid curves), in which $\bar{E}_T$ is dominant, agree rather well with the data. In particular, the structure function $\sigma_U$ begins to decrease as $-t$ becomes small, showing the effect of $\bar{E}_T$. In the model of Ref. [16] (dashed curves), $H_T$ is dominant, which leads to a large rise in the cross section as $-t'$ becomes small. Thus, in their parametrization, the relative contribution of $\bar{E}_T$ to $H_T$ appears to be underestimated. One can make a similar conclusion from the comparison between data and model predictions for $\sigma_{TT}$. This shows the sensitivity of the measured $\pi^0$ structure functions for constraining the transversity GPDs.

From Eq. (2) for $\sigma_T$ and Eq. (3) for $\sigma_{TT}$, one can conclude that $|\sigma_{TT}| < \sigma_T < \sigma_U$. One sees from Fig. 2 that $-\sigma_{TT}$ is a sizable fraction of the unseparated cross section while $\sigma_{LT}$ is very small, which implies that contributions from transversely polarized photons play a dominant role in the $\pi^0$ electroproduction process.

In conclusion, differential cross sections of exclusive pion electroproduction have been obtained in the few GeV region over a wide range of $Q^2$, $x_b$, and $t$. While the general features of $\pi^0$ electroproduction have been

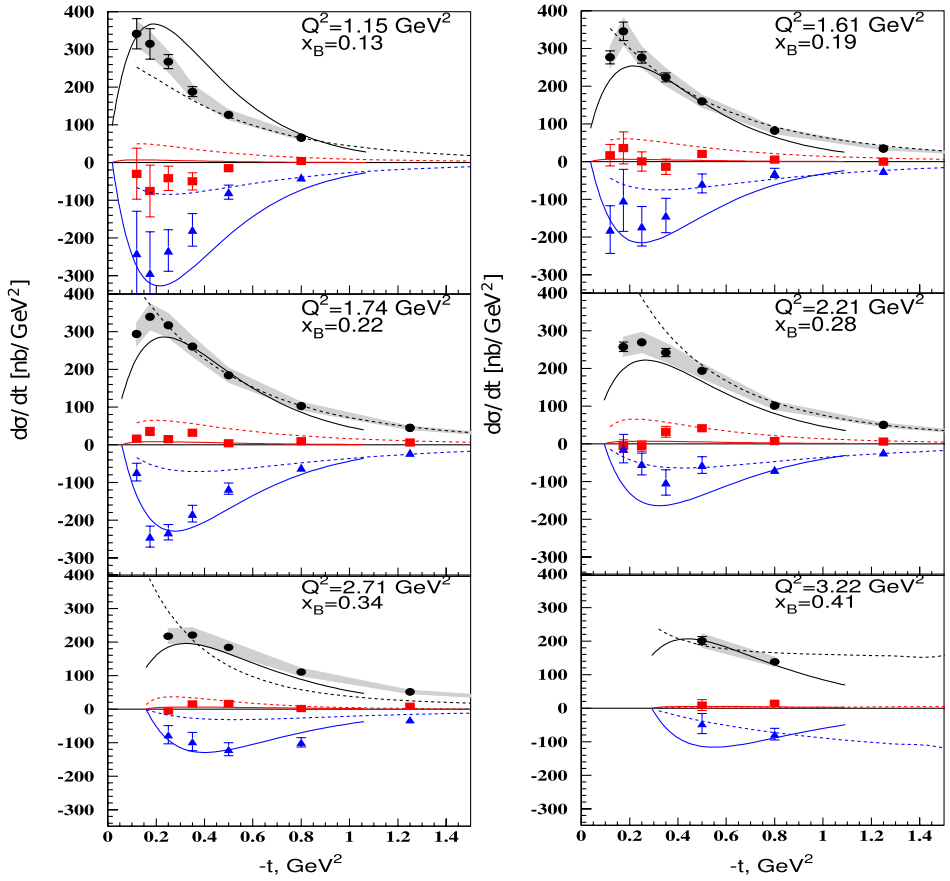


FIG. 2 (color online). The extracted structure functions vs $t$ for the bins with the best kinematic coverage and for which there are theoretical calculations. The solid curves are theoretical predictions produced with the models of Ref. [15] and the dashed are from [16]. The data and curves are as follows: the positive value circles (black) and curves are $\sigma_U (= \sigma_T + \epsilon\sigma_L)$, the negative value triangles (blue) and curves are $\sigma_{TT}$, and the squares (red) with accompanying curves are $\sigma_{LT}$. The shaded bands reflect the experimental systematic uncertainties.

described by recent Regge models [1,2], the focus of this Letter is on the handbag mechanism in terms of quark and gluon degrees of freedom. Within the handbag interpretation, the data appear to confirm the expectation that pseudoscalar and, in particular, $\pi^0$ electroproduction is a uniquely sensitive process to access the transversity GPDs $\bar{E}_T$ and $H_T$. The measured unseparated cross section is much larger than expected from leading-twist handbag calculations. This means that the contribution of the longitudinal cross section $\sigma_L$ is small in comparison with $\sigma_T$. The same conclusion can be made in an almost model independent way from the comparison of the cross sections $\sigma_U$, $\sigma_{TT}$, and $\sigma_{LT}$ [17].

Detailed interpretations are model dependent and quite dynamic in that they are strongly influenced by new data as they become available. In particular, calculations are in progress to compare the theoretical models with the single beam spin asymmetries obtained earlier with CLAS [18] and longitudinal target spin asymmetries, which are currently under analysis.

In the near future, new data on $\eta$ production and ratios of $\eta$ to $\pi^0$ cross sections are expected to further constrain GPD models. Extracting $\sigma_L$ and $\sigma_T$ with improved statistical accuracy and performing new measurements with transversely and longitudinally polarized targets would also be very useful.

We thank the staff of the Accelerator and Physics Divisions at Jefferson Lab for making the experiment possible. We also thank G. Goldstein, S. Goloskokov, P. Kroll, J. M. Laget, and S. Liuti for many informative discussions and clarifications of their work, and for making available the results of their calculations. This work was supported in part by the U.S. Department of Energy and National Science Foundation, the French Centre National de la Recherche Scientifique and Commissariat à l'Energie Atomique, the French-American Cultural Exchange (FACE), the Italian Istituto Nazionale di Fisica Nucleare, the Chilean Comisión Nacional de Investigación Científica y Tecnológica (CONICYT), the National Research Foundation of Korea, and the UK Science and Technology Facilities Council (STFC). The Jefferson Science Associates (JSA) operates the Thomas Jefferson National Accelerator Facility for the United States Department of Energy under Contract No. DE-AC05-06OR23177.

*Present address: Institut de Physique Nucléaire ORSAY, Orsay, France.
†Present address: INFN, Sezione di Genova, 16146 Genova, Italy.
‡Present address: Università di Roma Tor Vergata, 00133 Rome, Italy.

[1] J. M. Laget, Phys. Lett. B **695**, 199 (2011).
[2] M. M. Kaskulov, K. Gallmeister, and U. Mosel, Phys. Rev. D **78**, 114022 (2008); M. M. Kaskulov, arXiv:1105.1993.
[3] M. Diehl, Phys. Rep. **388**, 41 (2003), and references within.
[4] P. Hoodbhoy and X. Ji, Phys. Rev. D **58**, 054006 (1998).
[5] K. Goeke, M. V. Polyakov, and M. Vanderhaeghen, Prog. Part. Nucl. Phys. **47**, 401 (2001).
[6] S. Ahmad, G. R. Goldstein, and S. Liuti, Phys. Rev. D **79**, 054014 (2009).
[7] S. V. Goloskokov and P. Kroll, Eur. Phys. J. C **65**, 137 (2010).
[8] A. Airapetian *et al.* (HERMES Collaboration), Phys. Lett. B **682**, 345 (2010).
[9] M. Diehl and P. Hagler, Eur. Phys. J. C **44**, 87 (2005).
[10] M. Gockeler *et al.*(QCDSF Collaboration and UKQCD Collaboration), Phys. Rev. Lett. **98**, 222001 (2007).
[11] B. A. Mecking *et al.*, Nucl. Instrum. Methods Phys. Res., Sect. A **503**, 513 (2003).
[12] A. Afanasev, I. Akushevich, V. Burkert, and K. Joo, Phys. Rev. D **66**, 074004 (2002).
[13] L. Hand, Phys. Rev. **129**, 1834 (1963).
[14] E. Fuchey *et al.*, Phys. Rev. C **83**, 025201 (2011).
[15] S. V. Goloskokov and P. Kroll, Eur. Phys. J. A **47**, 112 (2011).
[16] G. R. Goldstein, J. O. Gonzalez Hernandez, and S. Liuti, Phys. Rev. D **84**, 034007 (2011).
[17] P. Kroll (private communication).
[18] R. De Masi *et al.*, Phys. Rev. C **77**, 042201 (2008).